INFORMATICS JOURNALS
The Journal of Electrochemical Society of India, Volume 74, Issue (1&2), January – March 2025; pp. 40-47
ISSN (Print) : 0013-466X
ISSN (Online) : xxxx-xxxx
DOI: 10.18311/JESCI/2025/51177

Development of a Robust Superhydrophobic Corrosion-Resistant Ni-WS_2 Composite Coating by Electrodeposition

Revathy Sreekumar[1,2] and S.S. Sreejakumari[1,2*]

[1]Materials Science and Technology Division, CSIR–National Institute for Interdisciplinary Science and Technology (NIIST), Thiruvananthapuram - 695019

[2]Academy of Scientific and Innovative Research (AcSIR), Ghaziabad - 201002, India

Abstract

The demand for high-performance materials with enhanced surface properties has grown significantly in various industrial sectors, including aerospace, automotive, marine, and energy. In the present work, a robust, superhydrophobic Ni-WS_2 coating was successfully developed through a scalable single-step electrodeposition process. Scanning Electron Microscopic analysis of Ni-WS_2 coated substrate surface showed a protruding rough surface comprising micro-nano pyramidal and conical nodular structures. By optimizing WS_2 concentration and deposition parameters, a hierarchical surface with a higher Water Contact Angle (WCA) of 159° was achieved and the coating is superhydrophobic. Due to the combined effect of superhydrophobicity and barrier effect of WS_2, the composite coating demonstrated exceptional corrosion resistance in comparison to the bare mild steel substrate and pure nickel coated mild steel.

Keywords: Composite, Corrosion Resistance, Electrodeposition, Ni-WS_2, Superhydrophobic

1. Introduction

Material deterioration and excessive energy consumption are closely linked, especially in industries where the performance and longevity of materials are critical. It is estimated that approximately $2.5 trillion in losses occur annually due to corrosion and wear. Excessive energy consumption can have both economic and environmental implications, resulting in sustainability issues and degradation. Thus, improving energy efficiency is crucial for long-term economic development and to meet human needs. The demand for high-performance materials with enhanced surface properties has grown significantly in various industrial sectors, including aerospace, automotive, marine, and energy[1]. Components used in these industries often face wear, corrosion, and high friction. These challenges necessitate the development of advanced coatings capable of protecting surfaces and extending the service life of critical components[2]. In response, composite coatings have emerged as a promising solution, offering multi-functional capabilities by integrating diverse material properties.

Nickel-based coatings have gained considerable attention due to their excellent mechanical strength, corrosion resistance, and ease of deposition through electrochemical methods[3,4]. Super-hydrophobic materials with an intrinsic water Contact Angle (CA) larger than 150° and a Sliding Angle (SA) below 10° have drawn a lot of interest due to their unique properties, such as anti-icing[5], corrosion resistance[6], drag reduction and self-cleaning[7]. WS_2 is a well-known transition metal dichalcogenide with a unique layered structure that facilitates low friction due to weak van der Waals forces between its layers. Furthermore, WS_2 contributes to self-lubricating properties, making it an excellent candidate for applications where reducing friction is critical[8,9].

Ranganatha *et al.*[10] fabricated Ni-W-P-WS_2 composite coating by electroless plating and explored its friction and

*Email: sreejakumari@niist.res.in

corrosion resistance. Lecina *et al.*[11] incorporated inorganic fullerene-like WS_2 (IF-WS_2) within Ni matrix, resulting in a uniform and compact coating, with better mechanical properties and enhanced tribological performance. Polycrystalline WS_2 thin films were electrodeposited on conducting glass plates by galvanostatic route[12]. Cui *et al.*[13] developed a Ni-WS_2 self-lubricating composite coating with remarkable self-lubricity and a lower friction coefficient at a value around 0.01–0.03.

This paper focuses on the development of a robust, superhydrophobic corrosion-resistant Ni-WS_2 composite coating by electrodeposition. Only a few reports are available in the literature on the combined effect of superhydrophobicity and barrier effect of WS_2. The strategic incorporation of WS_2 particles into the nickel matrix aims to synergistically enhance the coating's performance. The dual-phase composition improves nickel's inherent corrosion resistance and mechanical strength. This study systematically investigates the development, characterization, and performance evaluation of Ni-WS_2 composite coatings. The outcomes of this work will provide valuable insights into the design of multi-functional composite coatings, contributing to advancements in surface engineering and material science. Additionally, the findings have the potential to address pressing challenges in industries where enhancing the durability and efficiency of critical components is paramount.

2. Materials and Methods

2.1. Materials

Nickel sulphate ($NiSO_4 \cdot 6H_2O$), Nickel chloride ($NiCl_2 \cdot 6H_2O$, 98%), and Boric acid (H_3BO_3, 99.5%) were purchased from Merck. Cetyltrimethylammonium bromide (CTAB, $CH_3(CH_2)_{15}N(Br)(CH_3)_3$) and Saccharin ($C_7H_5NO_3S$) were obtained from Alfa Aesar. Tungsten disulfide particles (WS_2, ≤ 1 μm) were supplied by Sigma-Aldrich. Stearic acid, $CH_3(CH_2)_{16}COOH$ was supplied by Hi-media laboratories. All the chemicals were of analytical grade and used without further purification.

2.2. Coating Preparation

Electrodeposition was carried out in an aqueous electrolyte of Ni Watts bath containing $NiSO_4 \cdot 6H_2O$, $NiCl_2 \cdot 6H_2O$, and H_3BO_3. WS_2 nanoparticles were dispersed in a Ni bath, along with CTAB and saccharin (Table 1). The Ni-WS_2 bath was kept at a pH of 4 - 4.5. WS_2 particles were dispersed using an ultrasonicator for 30 minutes.

Nickel plate (7 cm × 5 cm × 1 cm, 99.7 % purity) and mild steel substrate (SSM) (6 cm × 6 cm, purity ≥ 99.5 %) were used as anode and cathode, respectively. All the mild steel samples used for coating were ground using SiC papers ranging from 80 to 1000 grits, followed by degreasing in acetone and distilled water, ultrasonically cleaned, and dried in the oven. MS samples were further surface-activated by dipping in 0.01M HCl and 0.1M NaOH. The anode, Ni plate, was polished using SiC papers of grit 80 and 100. This was followed by degreasing in acetone and distilled water, and finally drying in the oven. Electrodeposition parameters, including current density (2–6A/dm^2), time (5–30 min), and stirring rate (400–600 rpm), were varied. The concentration of WS_2 was also varied in the range (1–5) wt% (Table 1). Finally, Ni-WS_2 was deposited at optimized conditions of current density of

Table 1. Experimental conditions for Ni-WS_2 coating over mild steel substrate

Electrodeposition parameters	Composition or parameter	Value	Optimised conditions
	$NiSO_4.6H_2O$	250 g/l	-
Plating solution	$NiCl_2.6H_2O$	45 g/l	-
	H_3BO_3	40 g/l	-
	Saccharin	3 g/l	-
	CTAB	0.5 g/l	-
	WS_2	1-5 wt%	3 wt%
Deposition conditions	Current density	2-6 A/dm^2	5 A/dm^2
	Temperature	60°C	-
	Time	5-30 minutes	30 minutes
	Stirring rate	400-600 rpm	400 rpm

5 A/dm^2 for 30 mins at a temperature of 60°C with a 400 rpm stirring rate and 3wt% concentration of WS_2. After the electrodeposition, the samples were cleaned in running distilled water, followed by ultrasonic cleaning for 5 minutes in ethanol to remove loosely adsorbed particles, and then subjected to further analysis. The coated sample was finally modified with the low surface energy material stearic acid (SA).

2.3. Characterization of the Coatings

The surface morphology and elemental analysis of the developed coatings were examined using Zeiss EVO 18 cryo-SEM (EDS attached). The phase composition of the samples was studied using X-ray Diffraction (XRD) via a Bruker D2 Phaser X-ray diffractometer with Cu - K_α radiation (λ = 1.5406 A°) in the 0-90° range. Coating thickness was measured using a thickness measurement gauge (Elcometer). Thickness measurements at five different locations of the coated sample were done, and the average value was taken. The wettability of the developed coatings was measured by a Goniometer (Data Physics, Germany). The water contact angle was calculated by taking the average of five measurements taken at various points on the same sample.

A CH Instruments electrochemical workstation (CHI608E, CH Instruments Inc.) equipped with a standard three-electrode cell was used for electrochemical impedance spectroscopy and potentiodynamic polarization studies at room temperature in 3.5 wt% NaCl solution. The coated specimen with 1cm^2 exposed surface area was used as the working electrode; saturated calomel and a platinum grid were taken as the reference and counter electrodes, respectively. The specimens were kept in the electrolyte for 20 min before the experiment to attain their stable Open Circuit Potential (OCP). The potentiodynamic scan was done at a rate of 1 mV/s from −250 mV to +250 mV of the OCP values. The corrosion potential (E_{corr} vs. SCE) and corrosion current density (i_{corr}) of each sample were obtained from the applied potential vs. current Tafel plot. The impedance measurements were performed using an AC signal with a perturbation of 5 mV at OCP in the frequency range of 100 kHz-0.01 Hz. ZsimpWin software fits the generated EIS plots to determine the electrochemical parameters. Numerous circuits were examined until the Chi-square value decreased to less than 9×10^{-4} or no further fitting improvement was observed.

3. Results and Discussion

3.1. Surface Morphology and Elemental Composition

SEM micrographs of pure Ni and Ni-WS_2 composite coating deposited on mild steel are given in Figure 1 (a-b) and Figure 1 (c-d), respectively. Both the coatings had a uniform surface without any defects such as pores and cracks. The addition of WS_2 will cause a change in the microstructure of the composite coating and make the surface rougher. The development of a rough surface is an important factor in the preparation of special super-wetting materials[14].

During the time of deposition, Ni ions are attracted to WS_2 particles due to the electrostatic interaction between positively charged Ni ions and negatively charged WS_2 particles[15]. Ni ions then begin to deposit on the WS_2 particles, forming a thin film. Ni ions will continue depositing and will start to grow in size and shape. WS_2 hinders the crystal growth and increases the nucleation sites for the reduction of Ni ions, which results in reduced grain size in the case of Ni-WS_2 composite coating. The Ni-WS2-coated MS possessed a protruding rough surface comprising micro-nano pyramidal and conical nodular structures. This type of structure can enhance the mechanical strength, adhesion, and electrochemical performance of the Ni-WS_2 composite coating. EDS shows the distribution of elements on the surface of Ni-WS_2-coated MS as in Figures 2 and 3, Ni, W and S elements are uniformly distributed on the surface of the composite coating, which indicates that WS_2 is successfully embedded in the Ni matrix.

3.2 X-ray Diffraction Studies

X-ray diffraction was employed to examine the phase composition of the coating. The XRD pattern of pure Ni-coated MS is shown in Figure 4(a). From the data, three peaks of Ni at 2θ corresponding to 44.32°, 51.77°, and 76.3° are assigned to (111), (200), and (220) Bragg reflections of the face-centered cubic (fcc) structure of metallic nickel[16]. The incorporation of WS_2 particles causes important microstructural changes, providing more nucleation sites. It also retards the growth of large Ni crystals, resulting in smaller grain sizes. Analyzing the XRD pattern of the Ni-WS_2-coated sample, distinct peaks are observed at 14° and 33°, corresponding to the (002) and (102) phases, respectively. This confirms

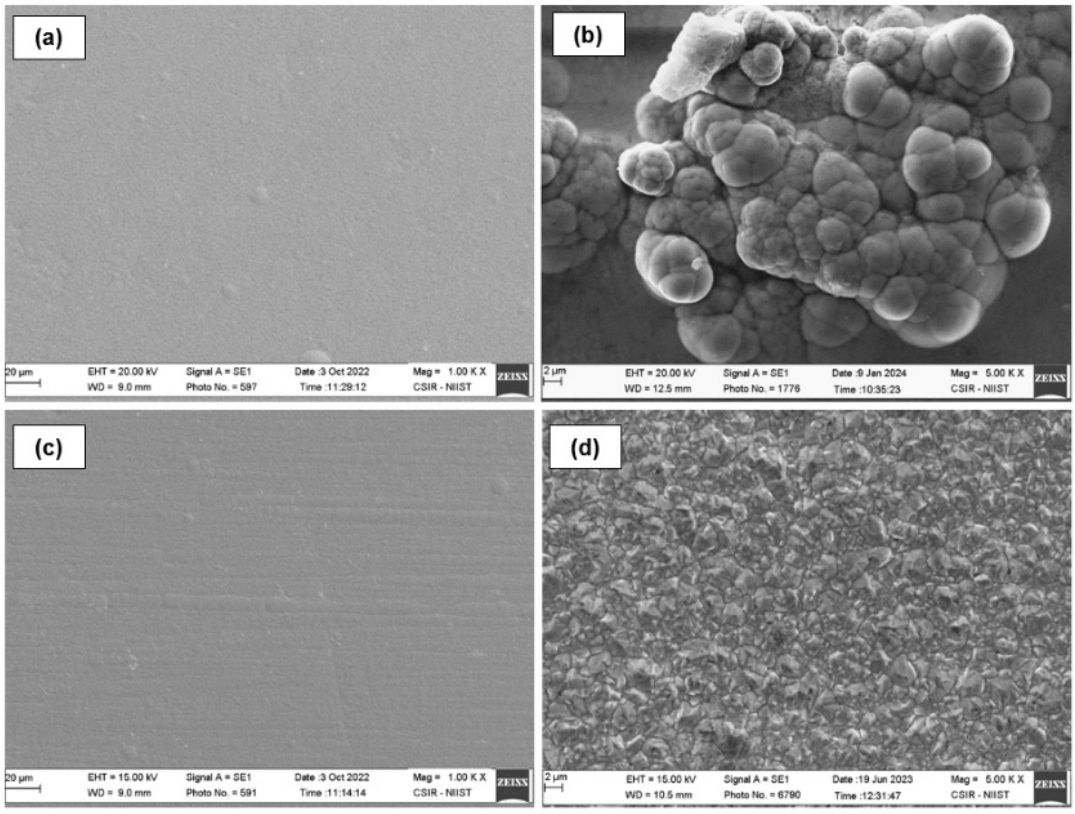
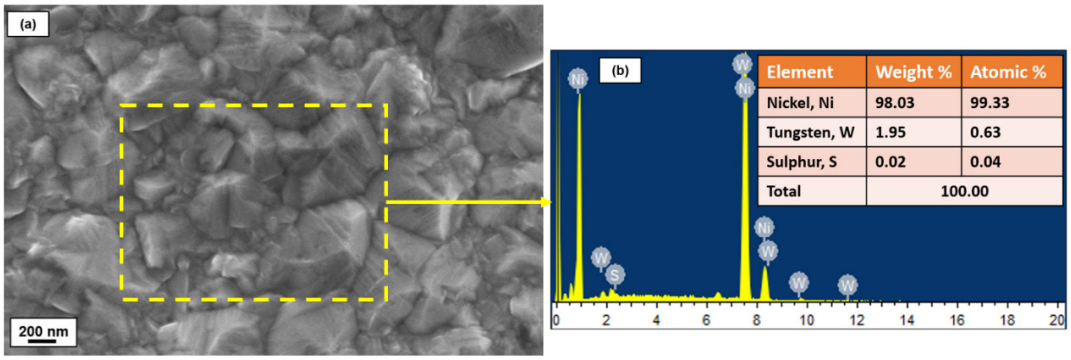


Figure 1. SEM micrographs of MS surface **(a)**-**(b)** Pure Ni coated, **(c)**-**(d)** Ni-WS_2 coated.



Element	Weight %	Atomic %
Nickel, Ni	98.03	99.33
Tungsten, W	1.95	0.63
Sulphur, S	0.02	0.04
Total	100.00	

Figure 2. **(a)**-**(b)** SEM-EDS of Ni-WS_2 coated MS surface.

the hexagonal closed-packed (hcp) structure of WS_2[17]. (Figure 4 (b)). Whenever Ni is deposited onto a substrate, the first few layers of atoms will tend to form the (111) plane[18]. The (111) plane is one of the most densely packed planes in a crystal lattice, and it has the lowest surface energy compared to other planes. Thus, the growth of the (111) plane helps to minimize the total surface energy of the crystal[19]. In this case, there is the presence of strong (111) Ni peaks indicating reduced surface energy. Post electrodeposition after treatment with SA it is believed that SA is chemically adsorbed on the Ni(111) surface via bi-dentate interaction, i.e., two oxygen atoms from the carboxylic acid group (-COOH) of stearic acid. This bonding interaction prevents the water molecules from forming hydrogen bonds with the surface, enhancing the hydrophobicity.

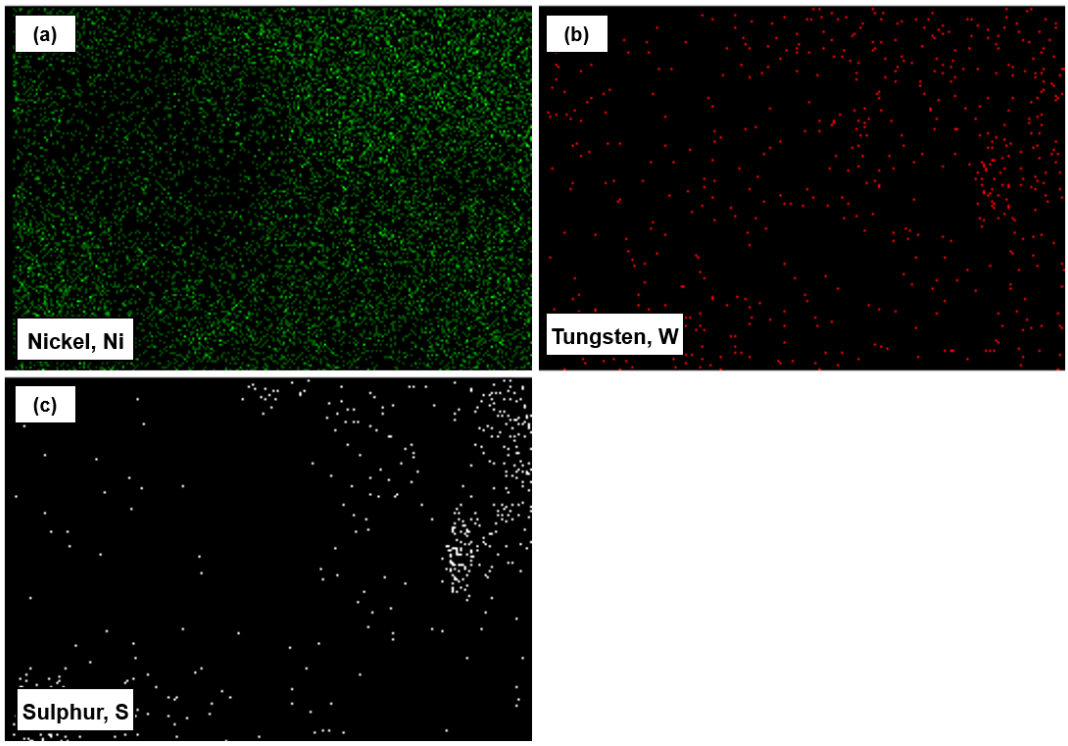


Figure 3. **(a)-(c)** Elemental mapping of Ni-WS_2 coating.

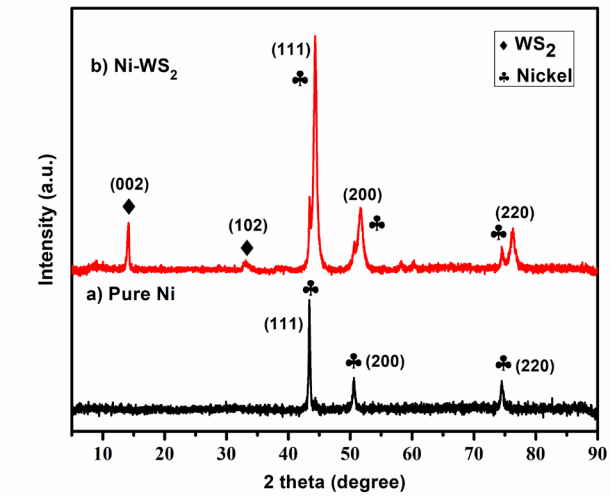


Figure 4. XRD pattern of (a) Pure Ni, (b) Ni-WS_2 coating.

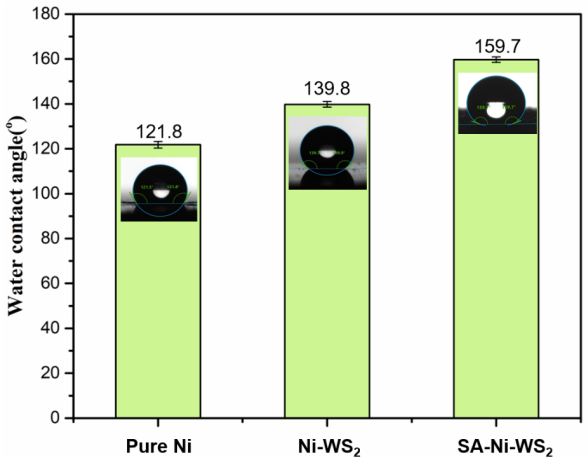


Figure 5. WCAs of coated sample (a) Pure Ni, (b) Ni-WS_2, (c) SA-Ni-WS_2.

3.3 Wettability Studies

Chemical composition, free energy of the surface, and surface morphology all affect the surface wetting property of a coating. Figure 5. shows the contact angle of the water droplet on the coated MS (pure Ni, Ni-WS_2, SA-Ni-WS_2). As it is evident from the WCA measurements, there was a gradual increase in the hydrophobicity of the surface (i.e. 121.8° to 159.7°). The water droplet remained on the surface of the Ni-WS_2-coated MS in an extremely spherical fashion. The micro-nanostructure, along with the action of low surface energy material SA (surface energy: 27.7 dynes/cm) reduces the contact area between the solid–liquid and water by forming a thin, strong cohesive layer on Ni-WS_2 coating.

Whenever applied over a surface, SA can self-assemble in an organized manner employing the hydrogen bonding of carboxyl groups as well as hydrophobic interactions in-between methyl groups. These hydrophobic chains create a barrier that prevents water from wetting the surface. As a result, water droplets tend to bead up and roll off the surface instead of spreading out and wetting it. The combined effect of hydrophobic surface chemistry and the roughness results in excellent superhydrophobic characteristics of the developed Ni-WS_2 coating.

3.4. Electrochemical Characterization

Figure 6. (a) shows the potentiodynamic polarization curves (Tafel plots) of samples by plotting the potential scanned from the cathodic region to the anodic region vs. the logarithm of current density. The values of corrosion current density (i_{corr}) and corrosion potential (E_{corr}), obtained by the extrapolation of cathodic and anodic sides, are given in Table 2. Variation of E_{corr} value towards a more positive direction, and the lower i_{corr} indicates the improved corrosion resistance of coatings, especially in the case of composite coatings. Presence of WS_2 in the coating leads to a substantial reduction in the i_{corr} value of Ni-WS_2 to 0.177 µA cm^{-2} from 4.143 µA cm^{-2} in the case of pure Ni and 17.110 µA cm^{-2} in the case of bare mild steel sample. The corresponding shift of the graph towards the left-hand side was observed. The reduction in i_{corr} values of the coated samples indicates the decreased ionic diffusion on the surface during the corrosion process. The Ni-WS_2 composite coating is more cathodic with respect to other samples and possesses excellent corrosion protection (E_{corr} MS: -0.678 V, Pure Ni: -0.417 V, Ni-WS_2: -0.246 V). The WS_2 incorporation has improved the corrosion resistance of the composite coatings by

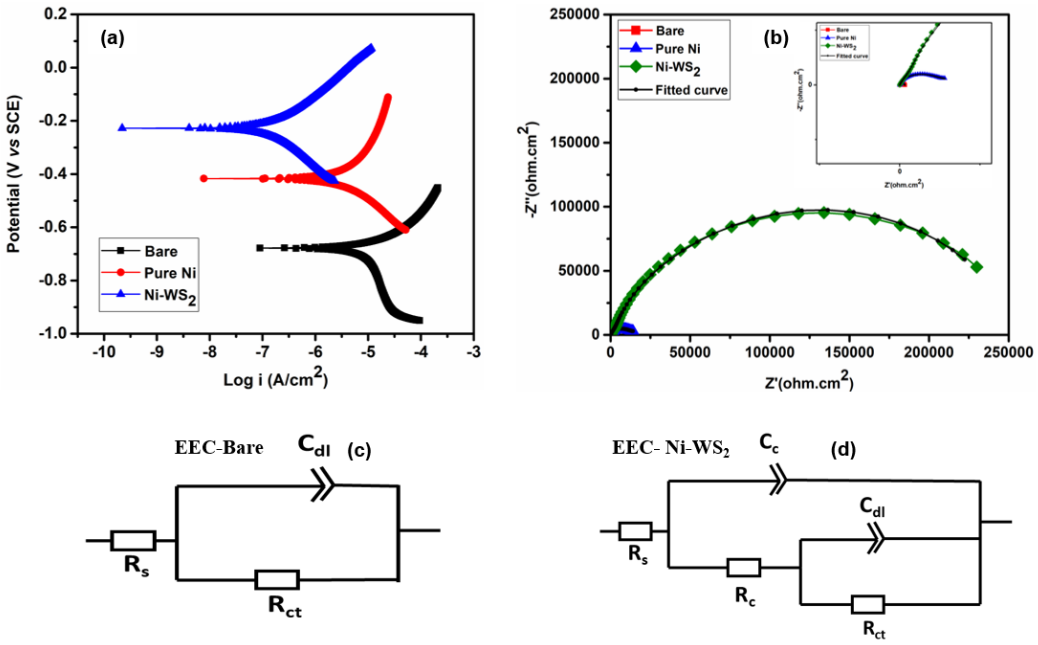


Figure 6. Electrochemical study for the Ni-WS_2 composite coatings **(a)** Tafel plot, **(b)** Nyquist plot, **(c)** EEC for the bare sample, **(d)** EEC for Ni- WS_2 coated sample.

Table 2. Electrochemical parameters obtained and corrosion inhibition efficiency of Ni-WS_2 coated samples

S/N	Substrate	Potentiodynamic polarisation				EIS	
		E_{corr} (V)	i_{corr} (µAcm^{-2})	η (%)	Corr.rate (mmpy)	R_{ct} (Ω cm^2)	η (%)
1.	Bare Mild Steel	-0.678	17.110	-	0.2013	3.955×10^2	-
2.	Pure Nickel	-0.417	4.143	75.78	0.0446	3.222×10^4	98.77
3.	Ni-WS_2	-0.246	0.177	98.96	0.0019	2.545×10^5	99.84

filling surface defects like tiny holes and porosities with WS_2 and acting as a barrier to corrosive ion diffusion. The even distribution of WS_2 in the deposit creates a passive layer between corrosive media and the deposited surface[20]. Thus, the corrosion rate (0.0019) of the Ni-WS_2 composite coating is exceptionally low compared to mild steel and pure Ni samples.

Electrochemical impedance spectroscopy measurements were performed in order to get a better understanding of the anticorrosive nature of coatings. Nyquist plots of bare mild steel, pure Ni and Ni-WS_2 composite coatings were obtained in 3.5% NaCl medium at the respective open circuit potentials (Figure 6 (b)). The Nyquist plots of all the samples have shown a single semi-circular arc in the investigated frequency region. The bare MS samples can be fitted with the circuit the equivalent electrochemical circuit (EEC) $R_s(C_{dl}R_{ct})$ (Figure 6 (c)), and all the coated samples are well fitted for the equivalent circuit of $R_s(C_cR_c(C_{dl}R_{ct}))$ (Figure 6 (d)).

R_s is the solution resistance, and R_{ct} and C_{dl} are the charge transfer resistance and double-layer capacitance, respectively. Instead of using pure capacitance due to the possibility of a dispersion effect between the metal/coating system, C represents a Constant Phase angle Element (CPE). The coating offered protection by the resistance element R_c. The parameters derived from electrochemical impedance measurements are summarized in Table 2. The results of the EIS studies also indicated a similar trend in the corrosion resistance that was observed in potentiodynamic polarization studies. The increased radius of the semicircular arc indicated the better anticorrosion property of the Ni-WS_2 composite coating than other samples. The superior value of R_{ct} obtained for the composite coating as offered more protection capability against corrosion.

4. Conclusions

A robust, superhydrophobic Ni-WS_2 coating was successfully developed through a scalable single-step electrodeposition process. SEM analysis of Ni-WS_2 coated substrate surface showed a protruding rough surface comprising micro-nano pyramidal and conical nodular structures. By optimizing WS_2 concentration and deposition parameters, a hierarchical surface with a higher Water Contact Angle (WCA) of 159° was achieved, and the coating is superhydrophobic. The composite coating demonstrated exceptional corrosion resistance in comparison to the bare mild steel substrate and pure nickel-coated mild steel, indicating its potential for industrial applications.

Acknowledgments

The first author, Revathy Sreekumar, is thankful to DST, Govt. of India, for the Inspire fellowship grant (IF 180987). The authors are grateful to Mr. Harish Raj and Ms. Anjali for their support in the characterization of the samples.

References

1. Davis JR. Surface engineering for corrosion and wear resistance. 2008; p 754. https://doi.org/10.31399/asm.tb.secwr.9781627083157.
2. Zhu S, Cheng J, Qiao Z, and Yang J. Tribol. Int. 2019; 133, 206–223. https://www.sciencedirect.com/science/article/pii/S0301679X18306169.
3. AM El-Sherik and Erb U. J. Mater. Sci. 1995; 30, 5743–5749. http://link.springer.com/10.1007/BF00356715.
4. Tenne R, Homyonfer M, and Feldman Y. Chem. Mater. 1998; 10, 3225–3238. https://pubs.acs.org/doi/10.1021/cm9802189.
5. Wang N, Xiong D, Deng Y, Shi Y, and Wang K. ACS Appl. Mater. \and Interfaces. 2015; **7**, 6260–6272. https://doi.org/10.1021/acsami.5b00558.
6. Boinovich LB *et al.,* Corros. Sci. 2012; 55, 238–245. https://www.sciencedirect.com/science/article/pii/S0010938X11005865.
7. Dong X *et al.*. Micromachines. 2020; 11, 159. https://www.mdpi.com/2072-666X/11/2/159.
8. Xu S *et al.,* Appl. Surf. Sci. 2014; 288, 15–25. http://dx.doi.org/10.1016/j.apsusc.2013.09.024.
9. Ouyang T, Lei W, Tang W, Shen Y, and Mo C. Wear. 2021; 204070, 486–487. https://www.sciencedirect.com/science/article/pii/S0043164821004567.
10. Ranganatha S, Venkatesha TV, and Vathsala K. Ind. Eng. Chem. Res.2012; 51, 7932-7940. https://pubs.acs.org/doi/10.1021/ie300104w.
11. García-Lecina E *et al.* Electrochim. Acta. 2013; 114, 859–867. http://dx.doi.org/10.1016/j.electacta.2013.04.088.
12. Devadasan JJ, Sanjeeviraja C, and Jayachandran M. J. Cryst. Growth. 2001; 226, 67–72. https://linkinghub.elsevier.com/retrieve/pii/S002202480100851X.
13. Cui S *et al.*, Rare Met. 2019; 38, 1078–1085. https://doi.org/10.1007/s12598-018-1152-5.
14. Kumari P, Chauhan P, and Kumar A. ACS Symposium Series. American Chemical Society.2022; 1408, 1–23. https://pubs.acs.org/doi/abs/10.1021/bk-2022-1408.ch001.

15. Shalom H *et al*., Chem. Phys. Lett.. 2020; 761, 138052. https://www.sciencedirect.com/science/article/pii/S0009261420309672.
16. Mohan S, Shriram S, and Karthikeyan S. Bull. Electrochem. 2002; 18, 241–246.
17. He Y, Sun WT, Wang SC, Reed PAS, and Walsh FC. Electrochim. Acta.2017; 245, 872–882. https://linkinghub.elsevier.com/retrieve/pii/S0013468617311866.
18. Zhou J *et al*.Appl. Surf. Sci.2019; 487, 1329–1340. https://doi.org/10.1016/j.apsusc.2019.05.244.
19. Jian-Min Z, Fei M, and Ke-Wei X. Chinese Phys. 2004; 13, 1082–1090. https://iopscience.iop.org/article/10.1088/1009-1963/13/7/020.
20. Liu B *et al*. Colloids surfaces a physicochem. Eng. Asp. 2022; 655, 130236. https://www.sciencedirect.com/science/article/pii/S0927775722019914.